

Piezo-Phototronic Effect on Selective Electron or Hole Transport through Depletion Region of Vis–NIR Broadband Photodiode

Haiyang Zou, Xiaogan Li, Wenbo Peng, Wenzhuo Wu, Ruomeng Yu, Changsheng Wu, Wenbo Ding, Fei Hu, Ruiyuan Liu, Yunlong Zi, and Zhong Lin Wang*

Silicon underpins nearly all microelectronics today and will continue to do so for some decades to come. However, for silicon photonics, the indirect band gap of silicon and lack of adjustability severely limit its use in applications such as broadband photodiodes. Here, a high-performance p-Si/n-ZnO broadband photodiode working in a wide wavelength range from visible to near-infrared light with high sensitivity, fast response, and good stability is reported. The absorption of near-infrared wavelength light is significantly enhanced due to the nanostructured/textured top surface. The general performance of the broadband photodiodes can be further improved by the piezo-phototronic effect. The enhancement of responsivity can reach a maximum of 78% to 442 nm illumination, the linearity and saturation limit to 1060 nm light are also significantly increased by applying external strains. The photodiode is illuminated with different wavelength lights to selectively choose the photogenerated charge carriers (either electrons or holes) passing through the depletion region, to investigate the piezo-phototronic effect on electron or hole transport separately for the first time. This is essential for studying the basic principles in order to develop a full understanding about piezotronics and it also enables the development of the better performance of optoelectronics.

Extensive applications of photodiodes in communication systems, medical, thermal imaging, environmental monitoring, and defense technology^[1–8] have increased the need for high-speed, sensitive broadband photodetectors. Silicon is the most

used semiconductor for discrete devices and integrated circuits, on account of the excellent compatibility with integrated circuits and fast development of nanofabrication techniques and nanomaterials.^[9–11] However, for silicon photonics, because of its weak absorption over the wavelength band 0.9 μm due to the indirect absorption mechanism^[12,13] and highly reflective surface across the electromagnetic spectrum,^[14] Si-based broadband photodiodes indicate an unsatisfactory response to wide wavelength range of lights.

Most of the reported silicon-based nano-/microsensors are still suffering from difficulties of further improving the responsivity and lack of adjustability. Piezo-phototronics is an effective approach to tune/modulate the charge carrier generation, separation or recombination, transport of electron–hole pairs at the interface/junction by the piezoelectric potential. The piezoelectric potential is generated due to dipole moments caused

by strains in a non-centrosymmetric wurtzite semiconducting crystal.^[15–18] Significant improvements have been demonstrated on the performance of solar cells,^[19] photodiodes,^[20,21] light-emitting diodes (LED),^[22,23] and even electrochemical processes and energy storages.^[24] Although, extensive investigations in piezotronic and piezo-phototronic effects in both theoretical analysis and device applications have been carried out, the tuning effects are studied based on the charge carriers of both electrons and holes in the depletion region. In order to develop a full understanding of the theory of piezotronics and enable the development of a high-performance electronics, optoelectronics, smart microelectromechanical systems (MEMS)/nanoelectromechanical systems (NEMS), and human–machine interfacing, it is essential to investigate how the piezo-phototronic effect influences on the electron or hole transport at the interface separately, and how these affect the performance.

Here, we fabricated high-performance broadband photodiodes based on p-Si and vertical ZnO nanowire (NW) array heterojunction operating in the wide range of lights from visible to near-infrared (NIR) wavelengths. The performances are significantly enhanced by applying the piezo-phototronics effect because of the modification of the interface properties at the Si/ZnO heterojunction. The enhancement of responsivity could

H. Zou, Dr. X. Li, Dr. W. Peng, Dr. R. Yu, C. Wu, Dr. W. Ding, F. Hu, R. Liu, Dr. Y. Zi, Prof. Z. L. Wang
School of Materials Science and Engineering
Georgia Institute of Technology
Atlanta, GA 30332-0245, USA
E-mail: zlwang@gatech.edu

Dr. X. Li
School of Electronic Science and Technology
Institute for sensing Technologies
Dalian University of Technology
Dalian, Liaoning 116024, China

Dr. W. Wu
School of Industrial Engineering
Purdue University
West Lafayette, IN 47907-2023, USA

Prof. Z. L. Wang
Beijing Institute of Nanoenergy and Nanosystems
Chinese Academy of Sciences
Beijing 100083, China

DOI: 10.1002/adma.201701412

reach a maximum of 78% for 442 nm illumination, and 18% for 1060 nm illumination. The linearity and saturation limit of 1060 nm light detection are significantly increased by applying external strains. Our results show that the fabricated p-Si/n-ZnO nanowire array heterojunction photodiodes have high sensitivity, fast response, and great stability, which are entirely suitable for operating at relatively high-speed response conditions in wide spectral bandwidth for various applications, such as nanorobotics, imaging, medical, analytical fields, optical-fiber communication systems.^[3] Furthermore, by employing two different wavelength of lights, electron-hole pairs are excited only on one side of the depletion region so as to restrict the kind of carriers (either electrons or holes) flowing across the interface of p-n junction in the depletion region. In this way, the type of the charge carriers could be controlled at the interface of p-n junction, thus the piezo-phototronic effect on the transport of either electrons or holes could be studied separately. The strain effect on the response time of the photodiodes is also studied in a systematic manner. These are all important and essential to study the basic principles to develop a full understanding of the theory of piezotronics and enable the development of the better performance of optoelectronics, such as solar cell, light emission diodes, and so on.

The structure of p-Si/n-ZnO broadband photodiode is schematically illustrated in **Figure 1a**. A piece of p-type Si wafer (about 10 mm × 10 mm) was cleaned by acetone, isopropyl

alcohol, and deionized water, and then was dried via a nitrogen gas gun. A thin seed layer (100 nm) of ZnO was sputtered on the silicon wafer, for hydrothermal growth of ZnO nanowire arrays at 95 °C for 90 min with diameters of 70–100 nm and length of ≈2 μm. Figure 1b shows the top view of ZnO nanowire arrays on a large scale to demonstrate the uniformity of the ZnO nanowire arrays. As indicated in Figure 1c, the samples have a strong X-ray diffraction (XRD) peak at $2\theta = 34.5^\circ$, corresponding to the (0002) plane of Wurtzite ZnO, which is responsible for the piezoelectric property. The ZnO nanowires have a high degree of alignment and are grown along +*c*-axis on (100) plane of Si substrate. Then, the samples were annealed at 350 °C for 2 h. If the indium tin oxide (ITO) electrode was directly deposited, the ITO could go deeper into the bottom through the gaps between the nanowires, and contact with p-Si or seed layer, causing short circuit and current leakage. To avoid these, a special design of a mushroom-like ceiling top electrode is proposed. ZnO nanowire arrays were first fully encapsulated by a layer of poly (methyl methacrylate) (PMMA) via spin coating and etched by oxygen plasma for 4 min to expose the top tips of the nanowires. The side-view and 30° tilt view scanning electron microscope (SEM) images (Figure 1d,e) show that the tips of ZnO nanowires were exposed. ITO with the thickness of ≈100 nm was deposited on the exposed tips of the nanowires to create core-shelled ZnO/ITO and flat PMMA plane to form a continuous ITO film. The top electrode has a mushroom-like

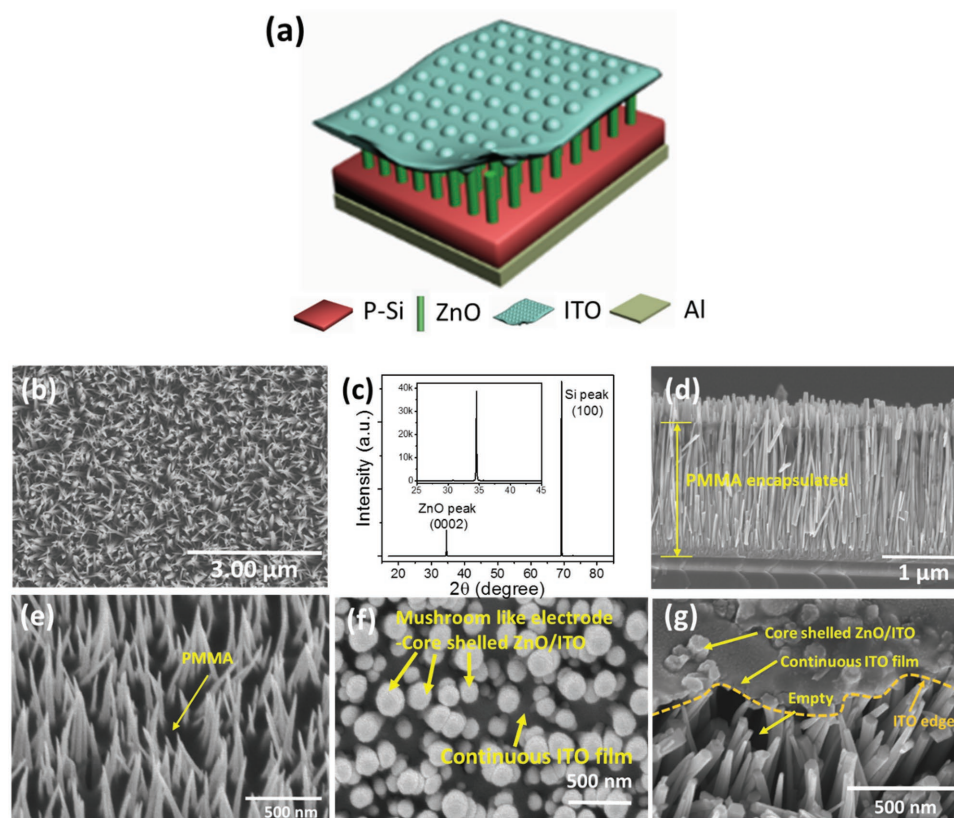


Figure 1. Device fabrication. a) Schematic structure of a p-Si/n-ZnO NW photodetector. SEM images of n-ZnO nanowires from b) top view before PMMA spin coating, c) XRD diffraction pattern obtained from the ZnO/p-Si heterostructure, d) side view and e) 30° tilt view of p-Si/n-ZnO heterojunction after PMMA spin coating and oxygen etched, f) ITO coating as top electrode. g) 30° tilt view of ITO coating at the edge of the device after applying strains repeatedly.

nanostructured surface as the top surface and a flat surface at the bottom. Figure 1f illustrates that the sharp tips of the nanowires are rounded (like the head of a mushroom), and are fully core-shell covered by ITO, and connected with each other via continuous ITO film. More details can be found in the Supporting Information. Aluminum was deposited on the back of p-Si wafer as the bottom electrode. Devices were cleaned by acetone to remove the PMMA, and then were heated to 350 °C again to burn out all PMMA residues, building up better Al-Si contact, and improving the transmission of ITO. Figure 1g shows the 30° tilt view SEM image of the edge of the device after applying compressive strains repeatedly. The PMMA was all removed, leaving the empty space between the nanowires. The continuous ITO film is supported by nanowires. We have found that the contact was firm and the nanowires showed the necessary flexibility, even when the p-Si substrate was cracked due to the excessive compressive strain, the ITO electrode and nanowires were not damaged or broken. Thus, the mushroom-like ceiling top transparent electrode was formed. It provides a novel method for fabricating top electrodes for nanowire arrays, allows for annealing at high temperature for nanowire arrays, and eliminates the direct contact of the top electrode and bottom layer. Such a special design was later found to significantly contribute to a low dark current, high rectifying ratio, and high light absorption. Detailed fabrication procedures and measurement setup are described step by step in the Experimental Section and Figures S1–S3 and Note S1 (Supporting Information).

Silicon has a weak absorption of the light over the wavelength of 0.9 μm due to the indirect absorption mechanism.^[12] For this hybridized broadband photodiode, the absorption in this region was greatly enhanced due to the nanostructured/textured top surface of ZnO and ITO (Figure 2a). The mushroom-like ceiling ITO electrode has a textured structure top surface that acts as an antireflection coating layer to reduce the reflection of NIR light, and it also has a flat surface at the bottom to enhance the reflection so that light could be reflected back again to be absorbed. To illustrate the photoresponse of different materials, a reference sample of ZnO nanowire arrays was grown on a glass (2 μm thick) with the same preparation conditions. The absorption spectra (Figure 2a) and transmission spectra (Figure 2b) show that n-ZnO nanowires are transparent to 1060 nm wavelength light because photons have less energy ($h\nu < E_g$) than the band gap needed to generate electron-hole pairs in ZnO; because of the local defect levels within the band gap,^[16,25–27] the ≈2 μm thick ZnO nanowire arrays absorb most of 442 nm wavelength light, the light intensity is greatly reduced when the light transmitted through the ZnO nanowires and the part (<4%) absorbed by p-Si are negligible. To further verify the intensity of the two different wavelength lights passing through the ≈2 μm ZnO, a power meter was used to measure the power density of light passed through the reference sample with/without ZnO NW arrays (Table S1, Supporting Information). The results are very similar to the data in Figure 2a.

Figure 2c shows the I - V characteristic of the broadband photodiode in dark (black line), under the illumination of 442 nm (red line) and 1060 nm (purple line) with power densities of 26.45 and 18.9 mW cm⁻², respectively. The photodiode

presents a typical rectifying characteristic of a p-n junction diode between -2 and 2 V. Figure 2d shows the sensitivity of the device measured under photoconductive mode at a reversed bias of -2 V, under different power densities of illumination. The sensitivity defined as $(I_{\text{light}} - I_{\text{dark}})/I_{\text{dark}}$ ^[28] is found to be about 5200% and 4000% (Figure 2d) at the power densities mentioned above. The photodiode still has a good sensitivity of 450% at low power densities of 0.3 mW cm⁻² for 1060 nm light, and 650% at 0.62 mW cm⁻² for 442 nm light.

The broadband photodiodes exhibit good photosensing properties under the illumination of lights at wavelengths ranged from 442 to 1060 nm at low power consumption (-2 V) (Figure 2e,f). The rise time, defined as the time interval for the response to rise from 10% to 90% of its peak value,^[12,29] is 1.071 ms under 442 nm light with 0.62 mW cm⁻² and 0.849 ms under 1060 nm light with 3.32 mW cm⁻² at the on-off frequency of 20 Hz. Similarly, the fall time, defined as the time interval for the response to decay from 90% to 10% of its peak value, is 1.304 ms for 442 nm light, and 1.277 ms for 1060 nm light, at the conditions mentioned above, respectively. The broadband photodiode has excellent stability and repeatability as shown in Figure 2e,f, as there is no observable deviation for more than 50 cycles.

Consequently, the results imply that the p-Si/n-ZnO heterojunction photodiodes have good performance, and are entirely suitable for operations at relatively high-speed conditions, as compared to other nanostructure photodiodes, as shown in Table 1 and some commercial silicon photodiodes.^[30,31] The excellent photoresponse characteristic of ZnO significantly attributes to some factors such as the presence of defect concentration in the ZnO grown, quality of ZnO nanowires, crystallographic orientation, and processing condition.^[32]

The piezo-phototronic effect was applied to modulate the optoelectronic processes and the performance as well. Under various strains, the broadband photodiode was first illuminated by 442 nm light, and then 1060 nm. I - V characteristics were measured under the high intensity of illumination with the power density of 26.5 mW cm⁻² of 442 nm light, then 18.9 mW cm⁻² of 1060 nm light, which are shown in Figure 3a,d. The amount of strain applied to the ZnO NWs is calculated based on Young's modulus ratio among different materials by assuming a uniform distribution of forces among each layer of the device for the state of mechanical equilibrium. Tensile strain is defined as positive and compressive strains as negative.^[22] The insets are the enlarged figures showing that under the above illumination conditions, the output current over various strains increases as the strains go higher from 0% to -1.42%. The intensity dependences of photocurrents ($|\Delta I| = |I_{\text{light}} - I_{\text{dark}}|$) under different strains are plotted in Figure 3b,e. When the samples are illuminated at 442 nm, the photocurrent rises as the strain increases between the power density of 0.6 and 26 mW cm⁻², as shown in Figure 3c. From Figure 3e, when the samples are illuminated at 1060 nm without strains, the photocurrent has a saturation limit at high power levels (above 16 mW cm⁻²) and that there are no additional photocurrent outputs from the photodiode as the incident optical power increases. By applying compressive strains, the device showed a better linearity and higher saturation limit, which demonstrate that the photoresponse is greatly enhanced

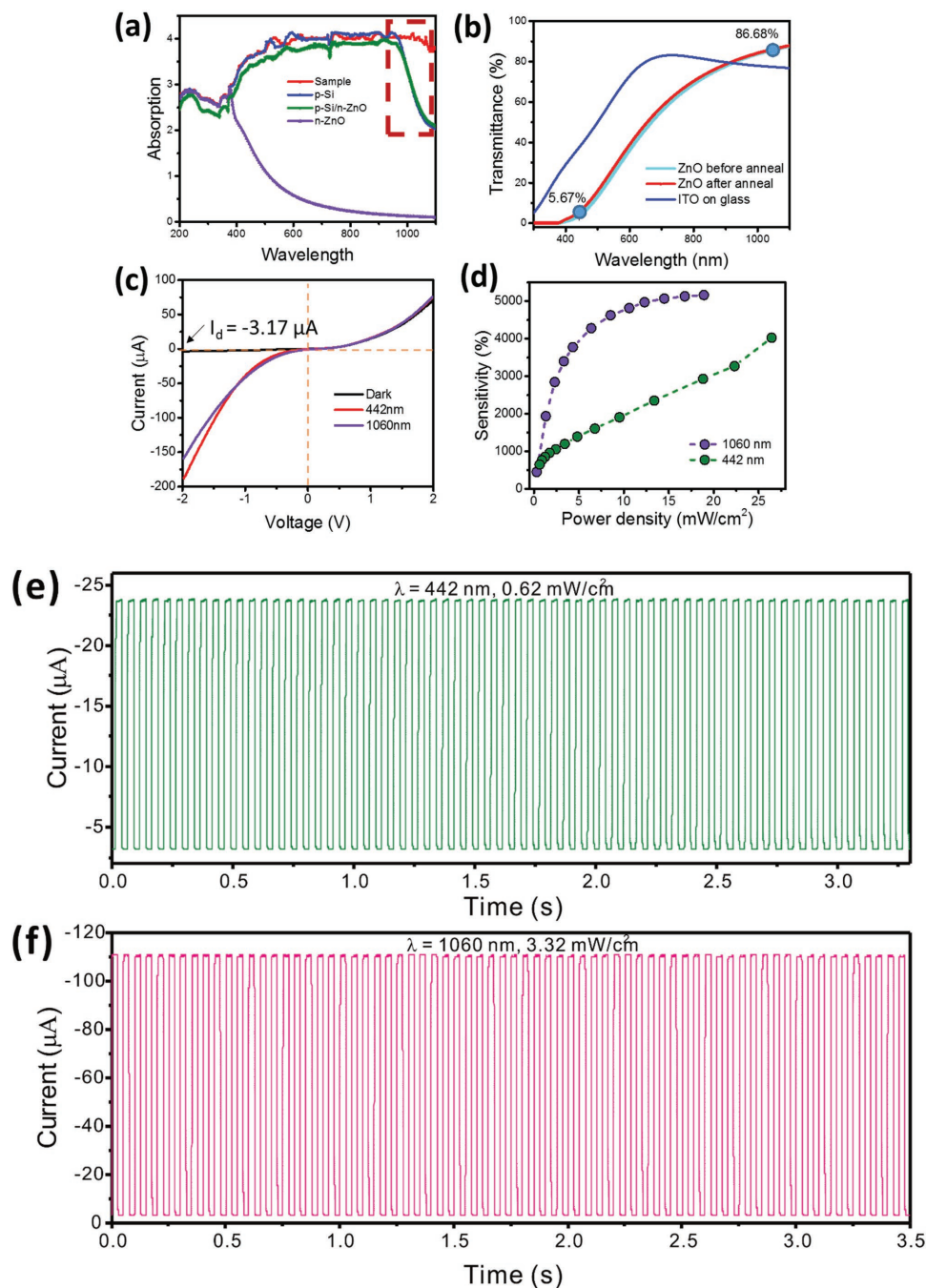


Figure 2. Optical properties of the device. a) Absorption spectra of p-Si, n-ZnO, p-Si/n-ZnO nanowire arrays without top electrode, and the sample with mushroom-like ceiling top electrode. b) Transmission spectra of ITO, ZnO NW array on the glass before annealing and after annealing. c) I - V characteristics of the device in dark, under the illumination 442 and 1060 nm wavelength with the power densities of 26.45 and 17.42 mW cm^{-2} , respectively. d) The sensitivity of the device under different illumination power densities. Repeatability and time response of the device under e) 442 nm light with a power density of 0.62 mW cm^{-2} and f) 1060 nm light with a power density of 3.32 mW cm^{-2} . The chopper on/off ratio is about 20 Hz. The devices were all measured at -2 V bias voltage.

(Figure S5, Supporting Information), even though the photocurrent decreases with the strains increased at low illumination power levels (below 6 mW cm^{-2} , Figure 3f). When the applied strain increases at high illumination power levels of 1060 nm light (above 10 mW cm^{-2}), the photocurrent increases. The turning point of photocurrent under compressive strains from

decreasing to increasing under the illumination of 1060 nm light is about 7 mW cm^{-2} . This is because the flowing free electrons at the interface would be trapped by local immobile piezoelectric positive charges at low intensity of illumination; while at high intensity of illumination, the large photocurrent would screen part of the piezoelectric potential (a dip is not

Table 1. A comparison of photosensing properties for various nanostructure photodiodes.

| Material and structure | Device type | Light of detection [nm] | Bias [V] | Dark current | Current | Rise time | Fall time | Reference |
|-------------------------------|--------------|-------------------------|----------|----------------------------|---|---------------------------------------|---|-----------|
| ZnO NW arrays/p-Si | p-n junction | 442–1060 | -2 | 3.17 μA | 131 μA (442 nm) 167 μA (1060 nm) | 0.97 ms (442 nm) 0.84 ms (1060 nm) | \approx 1.30 ms (442 nm) \approx 1.28 ms (1060 nm) | Our work |
| ZnO nanorods | M-S | 450 | - | 1 nA | \approx 25 nA | 3.7 s | \approx 60 s | [33] |
| ZnO hollow-sphere nanofilm | M-S | 350 | 5 | 50 nA | 2.6 μA | <5 ms | <5 ms | [34] |
| ZnS/ZnO | p-n junction | 320 | 1 | 0.2 μA | 1.0 μA | <0.3 s | \approx 1.7 s | [35] |
| ZnO NWs/i-MgO/n-Si | n-i-n | 365 | -5 | \approx 6.4 nA | \approx 8.6 μA | <160 ms | <350 ms | [36] |
| ZnO NW arrays/p-Si | p-n junction | 442 | 2 | 60 μA | 80 μA | 110–229 ms | 57 ms | [37] |
| TiO ₂ nanorod/p-Si | p-n junction | 405 | 3 | \approx 70 μA | \approx 140 μA | 9 ms | 9.7 ms | [38] |

created), so that the trapping force would be much lower, and the enhanced built-in field would be easier to promote electron transition from the p-side to the n-ZnO side. This will be further explained by band gap diagram in Figure 5.

The total responsivity of the photodiode, R , is defined as

$$R = \frac{I_{\text{light},s} - I_{\text{dark},s}}{P_{\text{ill}}} = \frac{\eta_{\text{ext}}}{h\nu} \Gamma_G \quad (1)$$

where $P_{\text{ill}} = I_{\text{ill}} \times S$ is the illumination power on the photodiode, $I_{\text{light},s}$ and $I_{\text{dark},s}$ represent the photon and dark current,

respectively, under the corresponding external strain, Γ_G is the internal gain, η_{ext} is the external quantum efficiency, q is the electronic charge; h is Planck's constant, ν is the frequency of the light; I_{ill} is the excitation power density, and S is the effective area of the photodiode. The photoresponsivity R is calculated as shown in Figure 4a,b for all the power density under various external strain conditions at the reverse bias of -2 V. When compressive strain increases at the 442 nm light, the responsivities of device increase. However, under the 1060 nm light, the responsivity decreases first and then increases with the turning point at about 6–8 mW cm^{-2} . The relative change

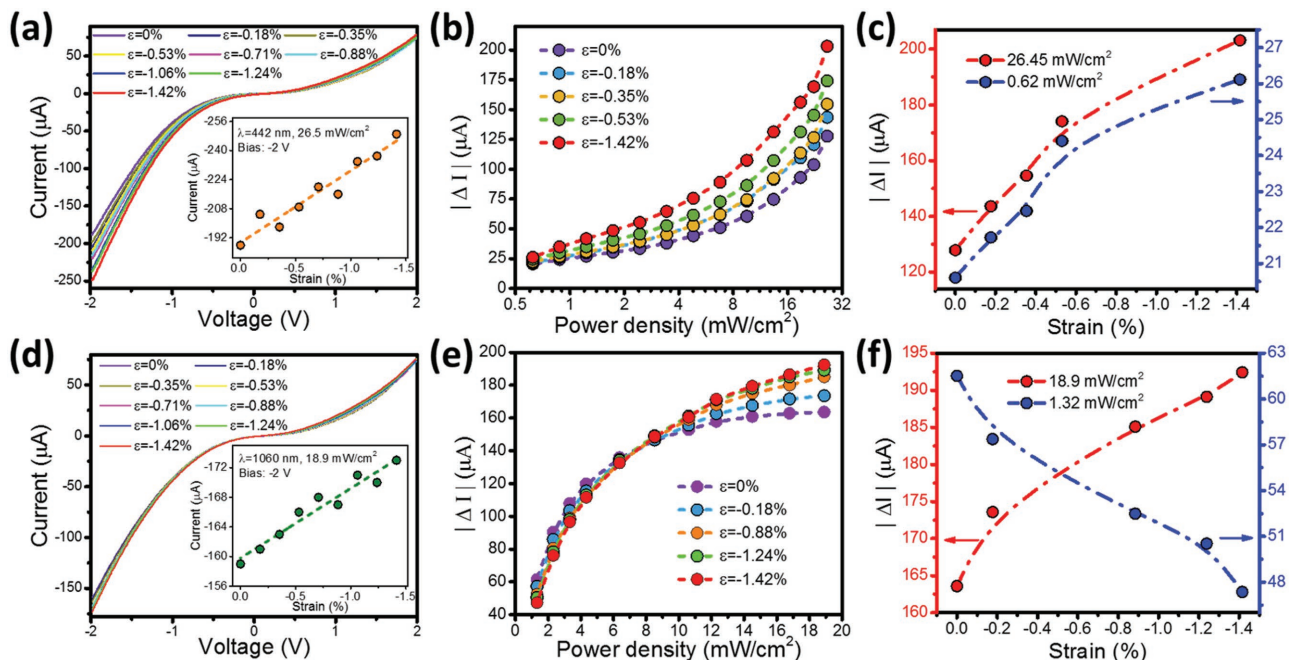


Figure 3. Piezo-phototronic effect on photoresponse. I - V characteristics of the device under illumination of a) 442 nm and d) 1060 nm wavelength with the power densities of 26.5, 18.9 mW cm^{-2} , respectively. The insets are the output current under different strains at -2 V bias voltage at the above illumination condition. Photocurrent of the device under b) 442 nm, e) 1060 nm under different strains and illumination conditions, biased at -2 V. c) The enlarged figure of photocurrent under different compressive strains at 442 nm light with relative high power densities of 26.45 mW cm^{-2} (red dots and dashed line) and 0.62 mW cm^{-2} (blue dots and dashed line). f) The enlarged figures of photocurrent under different compressive strains at 1060 nm light with a relatively high power density of 18.9 mW cm^{-2} (red dots and dashed line) and a low power density of 1.32 mW cm^{-2} (blue dots and dashed line).

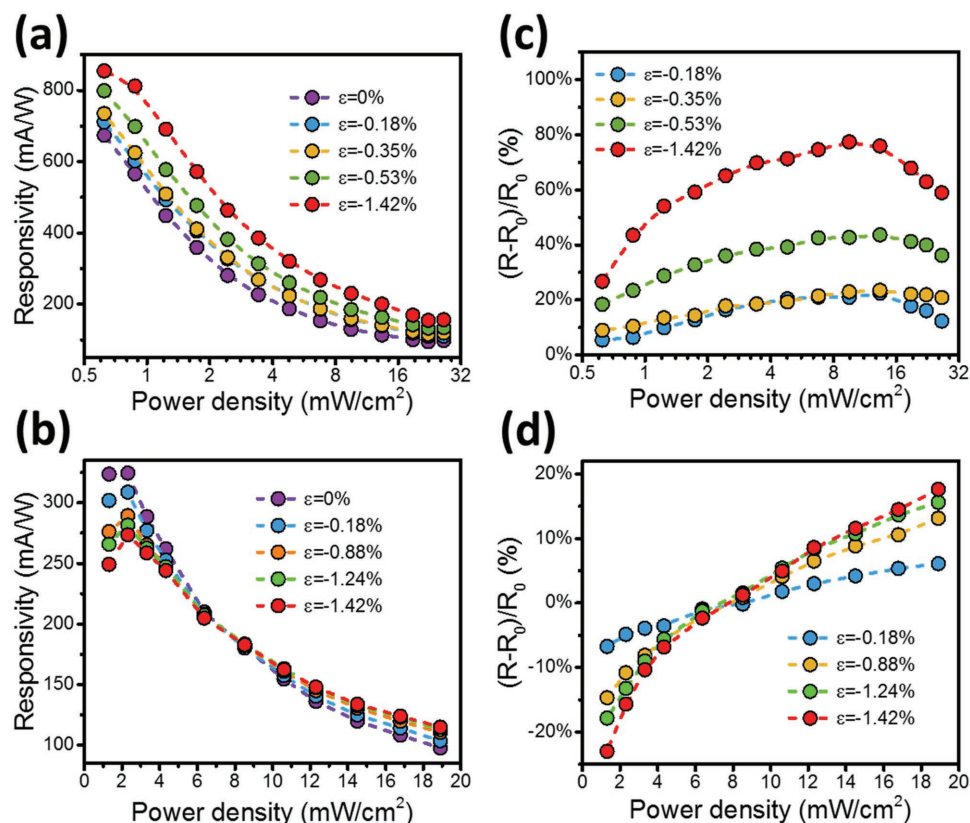


Figure 4. Piezo-phototronic effect on responsivity. a,b) Photoresponsivity and c,d) relative changes of photoresponsivity of the device under different strains and illumination conditions, biased at -2 V. (a, c) are under the illumination of 442 nm wavelength, and (b, d) are under the illumination of 1060 nm wavelength.

of responsivity is shown in the Figure 4c,d, which is defined as $(R - R_0)/R_0 \times 100\%$, where R is the responsivity under certain strain, and R_0 is the responsivity without strain. The enhancement can reach maximum 77.5% for 442 nm illumination, and 17.6% for 1060 nm illumination.

For a semiconductor p-n junction photodiode, the photogenerated charge carriers are normally generated in two active regions: the depletion layer and the diffusion regions.^[12] When the devices were illuminated at 442 nm at low power levels of illumination, the charge carriers were generated in the diffusion region near the surface (e.g., ZnO); while at high power levels, it would penetrate through the surface to a deep depth near or in the depletion layer. The 1060 nm wavelength light penetrates through the ZnO layer, and directly reaches the depletion layer on the p-Si side at the interface/junction. When the intensity of 1060 nm light increases, the active regions would also include the diffusion region. The electrons in the p-side diffusion region or the holes in the n-side diffusion region can reach the depletion by diffusion and then are swept to the other side by the internal field. The same is true for the minority carriers generated in the depletion region, as illustrated in Figure 5a.

The band diagrams of the p-Si/n-ZnO heterojunction broadband photodiode are shown with reversed biased voltage under the illumination of 442 nm (Figure 5b) and 1060 nm (Figure 5c) with external compressive strain based on Anderson's model.^[39] The band gap and electron affinity values for Si and electron

affinity values for Si and ZnO are $E_{g, Si} = 1.12$ eV, $\chi_{Si} = 4.05$ eV^[3] and $E_{g, ZnO} = 3.37$ eV, and $\chi_{ZnO} = 4.35$,^[40] respectively. There is a conduction band edge offset $\Delta E_c = 0.3$ eV and a valence band edge offset $\Delta E_v = 2.55$ eV.

As discussed above, the ≈ 2 μm ZnO nanowire arrays have almost a full absorption of 442 nm light and is completely transparent to 1060 nm light. Upon visible 442 nm wavelength light, electron-hole pairs are generated only in the n-ZnO region and the transport of free electrons and holes upon the electric field results in an increase of output current. Under such conditions, due to the electric field effect, only holes pass through the depletion regions, and electrons are directly migrated to the electrode side (Figure 5b, the red arrowhead is marked with a black cross, which means that few electrons flow across the interface in this case). Similarly, upon the illumination of 1060 nm light, electrons and holes are only generated on the p-Si side. No photoexcited holes transport through the depletion region to the p-Si side, instead they are directly collected at the electrode side under the applied bias (Figure 5c, the purple arrow is marked with a black cross, which means that no hole flows across the interface).

We now consider the case of strong illumination intensity of 442 or 1060 nm lights above ≈ 9 mW cm^{-2} , with the corresponding band structure shown as stage (i) in Figure 5b,c (dark dashed lines). When a compressive strain is applied along the c -axis of ZnO, positive polarization charges are induced within

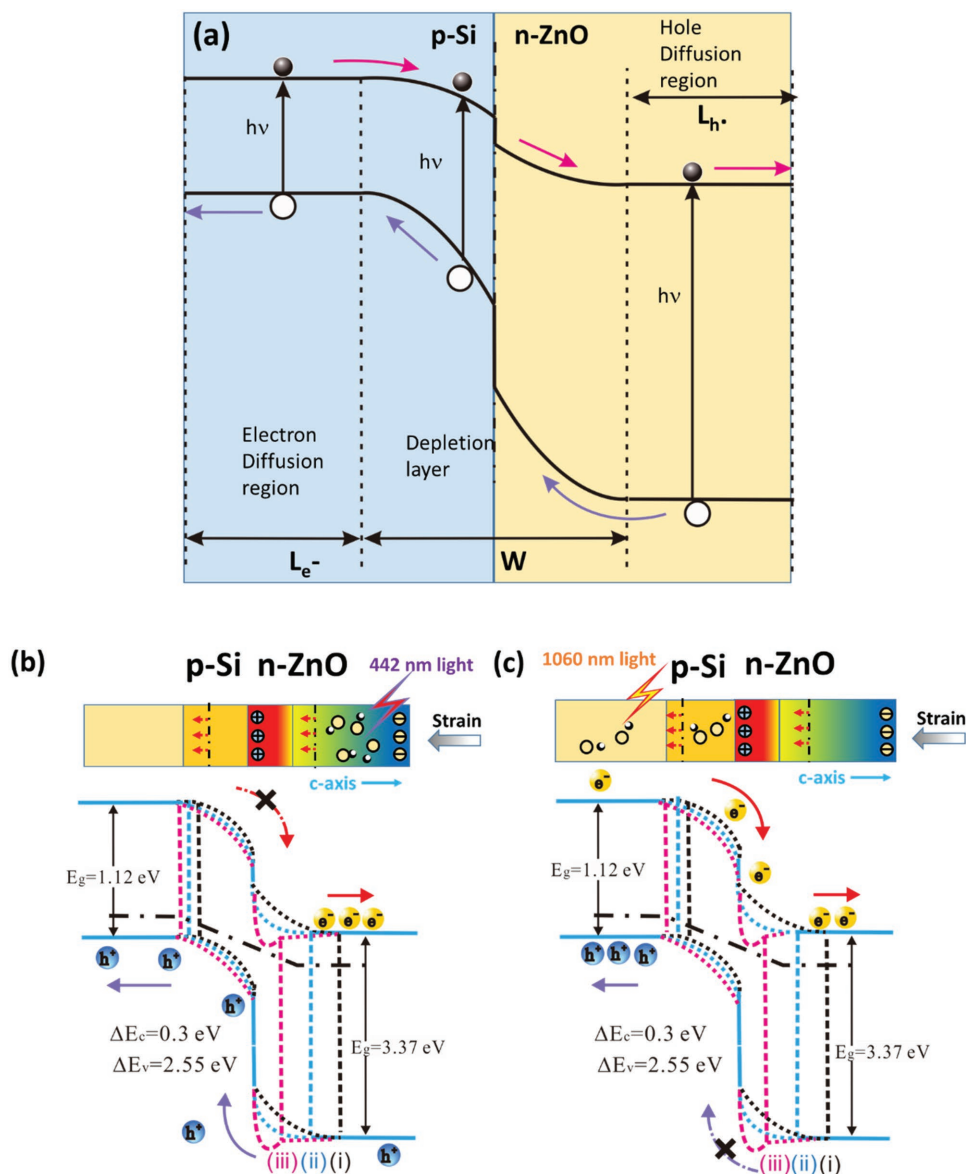


Figure 5. Working mechanism. a) Photoexcitation and energy-band diagram of the broadband photodiode. Schematic band diagrams of a p-Si/n-ZnO heterojunction under compressive strains applied to illustrate the working mechanism of piezo-phototronic effect under the illumination of b) 442 nm and c) 1060 nm wavelength. For the color gradient, pink represents positive potential and blue represents negative potential. The black, blue, and pink dashed lines show the energy band at different stages: (i) under high illumination without strains, (ii) high illumination with strains, and (iii) low illumination with strains.

the depletion region, the band structure is shown as stage (ii) in Figure 5b,c (light blue lines). The piezocharges will be mostly preserved without being screened by local residual free carriers, because the presence of depletion region can significantly enhance the piezoelectric effect. The conduction and valence bands in the junction region are lowered locally, the depletion layer will shrink on the n-type side and expand on the p-type side.^[39,41] Note, a dip is not created at the interface due to the screening effect of the light-induced electrons to the piezoelectric charges. As shown in Figure 5b,c, the edge of depletion shifts from the position of the black short dashed lines (stage (i)) to the position of blue dashed lines (stage (ii)), thus increasing the barrier height. It will strengthen the built-in field

and reduce the recombination that leads to having a higher collection probability for the carriers,^[19,28] leading to the increase of photocurrent; simultaneously, the responsivity is increased under compressive strain. Therefore, when strain is introduced under the high illumination intensity, the piezoelectric polarization on the n-ZnO side can effectively modulate the redistribution of charge carriers that leads to the increase of the photocurrent under the illumination of both 442 and 1060 nm lights.

In the case of weak illumination intensity of 442 or 1060 nm lights and under compressive strains (stage (iii)), less free electrons and holes are generated and accumulated, reducing the screening effect on the piezoelectrical potential, so that the strain induced polarization charges at the interface have a

stronger effect. This results in further downward bending in the local conductive valence band^[20] and shrink of the depletion region on the n-ZnO side. The positive piezopolarization charges will attract and trap some of the photogenerated electrons,^[16,39,41] which is equivalent to forming a dip at the interface.^[16,39,41] Consequently, it hinders the separation and reduces the photocurrent generated by the 1060 nm light (stage (iii), see the pink dashed curve in Figure 5c). The more strain applied, the larger positive piezopolarization charges displayed, and then more free electrons could be trapped. But for the carriers generated by the 442 nm light, the holes will not be trapped by the presence of the piezoelectric charges (stage (iii), see the pink dashed curve in Figure 5b), because they are both positively charged, and there is no attraction force between them.

Response time is mainly determined by the processes of the generation, separation, recombination, and transport of the charge carriers. Therefore, it is very critical to study the piezophototronic effect on the response time since it intimately correlates with these processes. For a given photodiode, the response time is most determined by t_{drift} , the charge collection time of the carriers in the depleted region of the photodiode and t_{diffused} , the charge collection time of the carriers in the diffusion region of the photodiode.^[3,12] The carriers have small mobility in n-ZnO, so when we consider the rise time and fall time, we would mostly focus on the n-ZnO side. The rise time is mostly dominated by the carriers' transport in the diffusion region (Notes S4 and S5, Supporting Information),^[12] the fall time here possibly depends on the minority carrier transit time in the depletion region (Notes S4 and S6, Supporting Information).^[12,29,42]

We measured the photoresponse under 442 and 1060 nm wavelength light illumination for about 50 cycles at the on-off frequency of 20 Hz under different light intensities. We calculate all cycles' response time and deviation, which is shown in Figure 6. From Figure 6a, under the illumination of 442 nm light from 0.62 to 3.42 mW cm⁻², the rise time rises from 1.2233 to 1.3493 ms when the compressive strain increases to 1.42%. Since it is under the relative low illumination power, the free charge carriers are mostly generated at the surface of ZnO (Note S2, Supporting Information). Electrons are directly collected at the surface, and the diffusion length of electron does not change, but the diffusion length of hole L_h increases because of the shrink of depletion layer on the n-ZnO side (see Figure 5b), which leads to the increase of fall time. From Figure 6b, the fall time drop by $\approx 5\%$ – 6% off as the strain increases to 1.42%. The physical model of Figure 5 indicates that when light is off, the holes remained in the depletion layer has less drift length on the n-ZnO side due to the depletion shift. Also, the strain induced positive polarization charges in the n-type region would repel the holes remaining on the p-Si side, which would provide an additional driving force to accelerate the hole migration to recombine and return to equilibrium state.

Figure 6c,d shows the rise time and fall time with various power densities under different strains, when the devices were under the illumination of 1060 nm. The rise time increases slightly when applied compressive strain increases. The induced positive polarization charges would cause trapping of electrons, and decelerate electrons moving from depletion to electrode. Also, the depletion width of the n-side shrink,

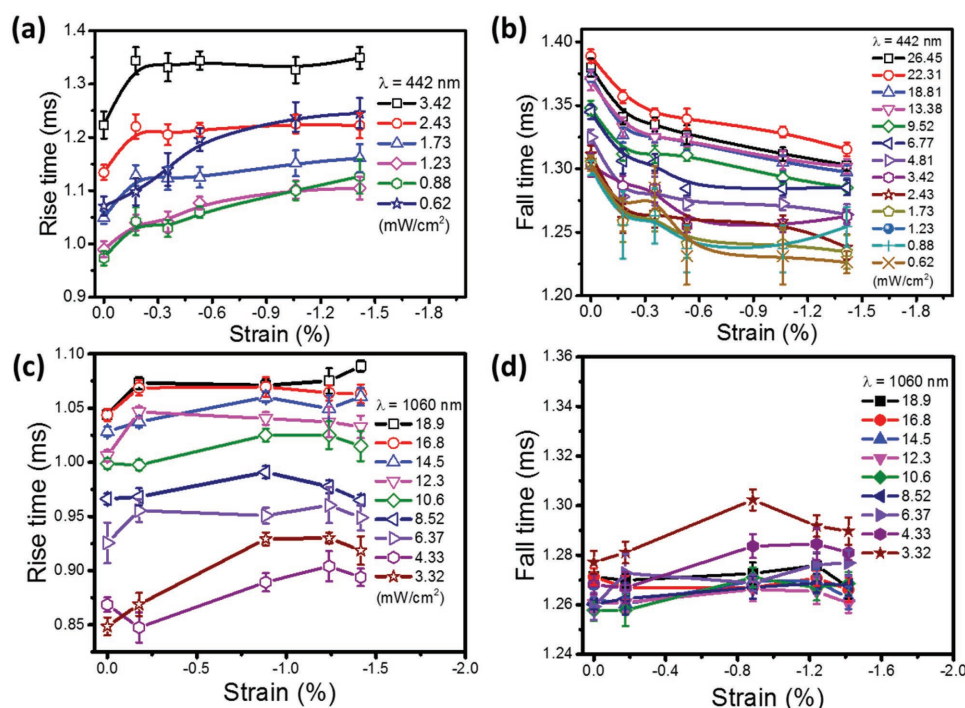


Figure 6. Response time under different compressive strains. The corresponding a) rise and b) fall time of the device under different compressive strains, under different power densities of 442 nm (unit: mW cm⁻²). The corresponding c) rise and d) fall time under different compressive strains under different power densities of 1060 nm light. The error bars indicate the range within a standard deviation.

resulting in the increase of the electron diffusion length. Both of these contribute to the increase of rise time. There are relatively small changes of fall time caused by strains when it was illuminated by 1060 nm light (Figure 6d). The electron drift length decreases because of the shift of the depletion region, which should reduce the response time. But on the other hand, the strain induced polarization positive charges attract the electrons from diffusing away from the depletion region (see Figure 5c). The two processes counteract against the other, so that the fall time has no significant change under various compressive strains.

In summary, we have developed high-performance broadband photodiodes based on p-Si/n-ZnO vertical nanowire arrays with high sensitivity, fast response time, and excellent stability in the wavelengths ranged from 442 to 1060 nm. The absorption in the near-infrared region is greatly enhanced due to the nanostructured/textured top surface, which breaks the material limit for Si photodiodes. Our broadband photodiodes are easy to be integrated into many existing schemes for light detection in many applications, such as imaging, environment monitor, light tractor, human-machine interfacing, defense technology, etc. The performances of the broadband photodiodes including the sensitivity, responsivity, linearity, saturation limit are enhanced significantly by the piezo-phototronic effect. The enhancement of responsivity can reach a maximum of 78% for 442 nm illumination, and 18% for 1060 nm illumination. The linearity and saturation limit of 1060 nm light detection are significantly increased by applying external strains. Moreover, we use different wavelength lights to selectively choose the excited charge carriers (either electrons or holes) that pass through the interface in depletion region, to investigate the effects of strain induced polarization charges on electrons or holes separately. We found that if the dip is created at the p-n heterojunction interface on the n-ZnO side due to the compressive strain induced positive piezopolarization charges, it would attract and trap some of the photogenerated electrons, but not holes. The influence of compressive strains on response time in different manners is also studied. These are critical for developing a more sophisticated piezotronic theory and broaden the scope of piezotronics and extend the framework for its potential applications.

Experimental Section

Fabrication Process of the p-Si/n-ZnO Photodiode: p-type Si wafer (100 mm B-doped (100) wafer, 1–10 Ω cm, 500 μ m SSP prime, UniversityWafer Inc.) was washed by ultrasonication with acetone, isopropyl alcohol, and distilled water, respectively, for 20 min. ZnO seed layer was deposited by Radio Frequency (RF) magnetron sputtering (PVD75 RF, Kurt J. Lesker Company) with a thickness of about 100 nm. The coated p-Si was then placed into mixed growth solution (25×10^{-3} M $\text{Zn}(\text{NO}_3)_2$, 12.5×10^{-3} M hexamethylenetetramine, and 0.8 M ammonium hydroxide) in a mechanical convection oven (Yamato DKN400, Santa Clara, CA, USA) at 95 $^\circ\text{C}$ for 90 min. The products were washed by isopropyl alcohol and distilled water, and dried in the oven at 60 $^\circ\text{C}$ for several hours. The samples were then annealed at 350 $^\circ\text{C}$ for 2 h. PMMA (MicroChem 495PMMA A8) was spin coated onto the samples, and then the samples were treated with oxygen plasma by Reactive Ion Etcher plasma system (Vision 320 RIE) for 4 min to expose the tips of ZnO nanowires. A thin layer of ITO was deposited on ZnO as the

top electrode and Al was deposited on p-Si as the bottom electrode. Samples were cleaned by acetone to remove the PMMA layer, and fired at 350 $^\circ\text{C}$ for 2 h in a compact rapid thermal processing tube furnace (RTP-1000D4, MTI Corporation). Testing wires were connected to the electrodes by silver paste.

Material Characterizations: Detailed microscopic structures of ZnO NWs were characterized by scanning electron microscope (Hitachi SU 8010).

Measurements: External strains were applied onto the sample by pressing the surface of the device on sapphire 2 fixed by layers of double-adhesive Kapton through a piece of sapphire 1 (Figure S3, Supporting Information) with a 3D mechanical stage (movement resolution ≈ 10 μ m). The device was fixed onto the sample holder through double-sided Kapton polyimide tape. Transmission and absorption spectra of materials were measured by a UV-vis spectrophotometer (JASCO V-630). *I-V* characteristics of the devices were measured and recorded by a computer-controlled measurement system with a Stanford SRS low noise current preamplifier (SR570)/SRS low-noise voltage preamplifier (SR560) in conjunction with a General-Purpose Interface Bus (GPIB) controller (GPIB-USB-HS, NI 488.2). The 442 nm wavelength optical input stimuli were provided by a He-Cd laser (model no. K157511-G, Kimmon Koha Co., Ltd.). The multichannel fiber coupled laser source was used for 1060 nm excitation. A continuously variable filter was used to control the light power density, which was measured by a thermopile power meter (Newport 818P-001-12). Chopper on-off frequency was about 20 Hz. The power density of light was measured by a power meter (Newport 1919-R).

Supporting Information

Supporting Information is available from the Wiley Online Library or from the author.

Acknowledgements

H.Z., X.L., W.P., and W.W. contributed equally to this work. H. Z. would like to thank the Georgia Tech IEN Department staff Chris Yang and Charlie Suh for the guidance and training on cleanroom equipment. The research was supported by the U.S. Department of Energy, Office of Basic Energy Sciences (Award DE-FG02-07ER46394), the National Science Foundation (DMR-1505319), and the “thousands talents” program for pioneer researcher and his innovation team, China.

Conflict of Interest

The authors declare no conflict of interest.

Keywords

broadband photodetectors, piezo-phototronic effect, p-Si/n-ZnO, visible/near-infrared, ZnO nanowire arrays

Received: March 13, 2017

Revised: April 24, 2017

Published online:

- [1] X. Gong, M. H. Tong, Y. J. Xia, W. Z. Cai, J. S. Moon, Y. Cao, G. Yu, C. L. Shieh, B. Nilsson, A. J. Heeger, *Science* **2009**, 325, 1665.
- [2] S. Middelhoeck, S. A. Audet, *Silicon Sensors*, Academic Press, London, UK **1989**.

- [3] S. M. Sze, K. K. Ng, *Physics of Semiconductor Devices*, John Wiley & Sons, New York, **2006**.
- [4] R. M. Yu, S. M. Niu, C. F. Pan, Z. L. Wang, *Nano Energy* **2015**, *14*, 312.
- [5] C. F. Pan, M. X. Chen, R. M. Yu, Q. Yang, Y. F. Hu, Y. Zhang, Z. L. Wang, *Adv. Mater.* **2016**, *28*, 1535.
- [6] J. Chen, Y. Huang, N. Zhang, H. Zou, R. Liu, C. Tao, X. Fan, Z. L. Wang, *Nat. Energy* **2016**, *1*, 16138.
- [7] H. Y. Zou, E. Gratz, D. Apelian, Y. Wang, *Green Chem* **2013**, *15*, 1183.
- [8] W. Z. Wu, X. N. Wen, Z. L. Wang, *Science* **2013**, *340*, 952.
- [9] V. R. Almeida, C. A. Barrios, R. R. Panepucci, M. Lipson, *Nature* **2004**, *431*, 1081.
- [10] M. Lipson, *J. Lightwave Technol.* **2005**, *23*, 4222.
- [11] H. Y. Zou, J. Chen, Y. N. Fang, J. L. Ding, W. B. Peng, R. Y. Liu, *Nano Energy* **2016**, *27*, 619.
- [12] J.-M. Liu, *Photonic Devices*, Cambridge University Press, Cambridge, UK **2005**.
- [13] M. A. Juntunen, J. Heinonen, V. Vähänissi, P. Repo, D. Valluru, H. Savin, *Nat. Photonics* **2016**, *10*, 777.
- [14] C. Wu, C. H. Crouch, L. Zhao, J. E. Carey, R. Younkin, J. A. Levinson, E. Mazur, R. M. Farrell, P. Gothoskar, A. Karger, *Appl. Phys. Lett.* **2001**, *78*, 1850.
- [15] Y. Hu, Y. Chang, P. Fei, R. L. Snyder, Z. L. Wang, *ACS Nano* **2010**, *4*, 1234.
- [16] M. X. Chen, C. F. Pan, T. P. Zhang, X. Y. Li, R. R. Liang, Z. L. Wang, *ACS Nano* **2016**, *10*, 6074.
- [17] W. Wu, L. Wang, R. Yu, Y. Liu, S. H. Wei, J. Hone, Z. L. Wang, *Adv. Mater.* **2016**, *28*, 8463.
- [18] W. Peng, R. Yu, X. Wang, Z. Wang, H. Zou, Y. He, Z. L. Wang, *Nano Res.* **2016**, *9*, 3695.
- [19] X. N. Wen, W. Z. Wu, Z. L. Wang, *Nano Energy* **2013**, *2*, 1093.
- [20] Q. Yang, X. Guo, W. H. Wang, Y. Zhang, S. Xu, D. H. Lien, Z. L. Wang, *ACS Nano* **2010**, *4*, 6285.
- [21] F. Zhang, Y. Ding, Y. Zhang, X. L. Zhang, Z. L. Wang, *ACS Nano* **2012**, *6*, 9229.
- [22] C. F. Pan, L. Dong, G. Zhu, S. M. Niu, R. M. Yu, Q. Yang, Y. Liu, Z. L. Wang, *Nat. Photonics* **2013**, *7*, 752.
- [23] C. F. Wang, R. R. Ba, K. Zhao, T. P. Zhang, L. Dong, C. F. Pan, *Nano Energy* **2015**, *14*, 364.
- [24] Y. Liu, Y. Zhang, Q. Yang, S. M. Niu, Z. L. Wang, *Nano Energy* **2015**, *14*, 257.
- [25] Z. Y. Fan, P. C. Chang, J. G. Lu, E. C. Walter, R. M. Penner, C. H. Lin, H. P. Lee, *Appl. Phys. Lett.* **2004**, *85*, 6128.
- [26] U. Schwing, B. Hoffmann, *J. Appl. Phys.* **1985**, *57*, 5372.
- [27] Y. F. Chan, W. Su, C. X. Zhang, Z. L. Wu, Y. Tang, X. Q. Sun, H. J. Xu, *Opt. Express* **2012**, *20*, 24280.
- [28] Z. L. Wang, *Piezotronics and Piezo-Phototronics*, 1st ed., Springer, New York **2013**.
- [29] B. E. Saleh, M. C. Teich, B. E. Saleh, *Fundamentals of Photonics*, Wiley, New York **1991**.
- [30] J. E. Carey, C. H. Crouch, M. Shen, E. Mazur, *Opt. Lett.* **2005**, *30*, 1773.
- [31] B. Franta, D. Pastor, H. H. Gandhi, P. H. Rekemeyer, S. Gradečak, M. J. Aziz, E. Mazur, *J. Appl. Phys.* **2015**, *118*, 225303.
- [32] P. Sharma, K. Sreenivas, K. V. Rao, *J. Appl. Phys.* **2003**, *93*, 3963.
- [33] S. E. Ahn, J. S. Lee, H. Kim, S. Kim, B. H. Kang, K. H. Kim, G. T. Kim, *Appl. Phys. Lett.* **2004**, *84*, 5022.
- [34] M. Chen, L. F. Hu, J. X. Xu, M. Y. Liao, L. M. Wu, X. S. Fang, *Small* **2011**, *7*, 2449.
- [35] L. F. Hu, J. Yan, M. Y. Liao, H. J. Xiang, X. G. Gong, L. D. Zhang, X. S. Fang, *Adv. Mater.* **2012**, *24*, 2305.
- [36] T. C. Zhang, Y. Guo, Z. X. Mei, C. Z. Gu, X. L. Du, *Appl. Phys. Lett.* **2009**, *94*, 113508.
- [37] Z. N. Wang, R. M. Yu, X. N. Wen, Y. Liu, C. F. Pan, W. Z. Wu, Z. L. Wang, *ACS Nano* **2014**, *8*, 12866.
- [38] A. M. Selman, Z. Hassan, M. Husham, N. M. Ahmed, *Appl. Surf. Sci.* **2014**, *305*, 445.
- [39] Y. Liu, S. M. Niu, Q. Yang, B. D. B. Klein, Y. S. Zhou, Z. L. Wang, *Adv. Mater.* **2014**, *26*, 7209.
- [40] A. Janotti, C. G. Van de Walle, *Rep. Prog. Phys.* **2009**, *72*, 126501.
- [41] W. Wu, Z. L. Wang, *Nat. Rev. Mater.* **2016**, *1*, 16031.
- [42] C. H. Chao, W. J. Weng, D. H. Wei, *J. Vac. Sci. Technol., A* **2016**, *34*, 02D106.